MAGNETIC FIELD INSTRUMENTS FOR THE FAST AURORAL SNAPSHOT EXPLORER

R. C. ELPHIC
Los Alamos National Laboratory, Los Alamos, New Mexico, U.S.A.

J. D. MEANS, R. C. SNARE, R. J. STRANGEWAY and L. KEPKO
Institute of Geophysics and Planetary Physics/UCLA, Los Angeles, California, U.S.A.

R. E. ERGUN
Laboratory for Atmospheric and Space Sciences, University of Colorado, Boulder, Colorado, U.S.A.

Abstract. The FAST magnetic field investigation incorporates a tri-axial fluxgate magnetometer for DC and low-frequency (ULF) magnetic field measurements, and an orthogonal three-axis searchcoil system for measurement of structures and waves corresponding to ELF and VLF frequencies. One searchcoil sensor is sampled up to 2 MHz to capture the magnetic component of auroral kilometric radiation (AKR). Because of budget, weight, power and telemetry considerations, the fluxgate was given a single gain state, with a 16-bit dynamic range of $\pm$65536 nT and 2 nT resolution. With a wide variety of FAST fields instrument telemetry modes, the fluxgate output effective bandwidth is between 0.2 and 25 Hz, depending on the mode. The searchcoil telemetry products include burst waveform capture with 4- and 16-kHz bandwidth, continuous 512-point FFTs of the ELF/VLF band (16 kHz Nyquist) provided by a digital signal processing chip, and swept frequency analysis with a 1-MHz bandwidth. The instruments are operating nominally. Early results have shown that downward auroral field-aligned currents, well-observed over many years on earlier missions, are often carried by accelerated electrons at altitudes above roughly 2000 km in the winter auroral zone. The estimates of current from derivatives of the field data agree with those based on flux from the electrons. Searchcoil observations help constrain the degree to which, for example, ion cyclotron emissions are electrostatic.

1. Introduction

The primary scientific thrust of the Fast Auroral Snapshot Explorer mission is to measure, characterize and understand rapidly changing and small scale microphysical processes associated with the aurora. Consequently the payload is designed to obtain very high-time resolution particle and fields measurements in low-altitude polar earth orbit. Measurements are made in the auroral zone between 350 and 4200 km altitude, and allow study of the plasma physics of auroral processes on length scales down to tens of meters. DC magnetic field measurements are essential for organizing particle distributions. They also provide an important large-scale backdrop for high sample rate and burst mode particles and fields observations. Magnetic field measurements in the auroral zone are critical for providing the instantaneous main earth's field for particle pitch-angles, for indicating the presence

Space Science Reviews **98:** 151–168, 2001.

of large- and small-scale field-aligned currents in the auroral zone and electromagnetic wave phenomena associated with auroral processes. The signatures of field-aligned currents are observed largely as east-west deflections in the background field, and are associated with north-south variations in the electric field at ionospheric altitudes (Sugiura *et al.*, 1982). This relationship was observed to hold down to the smallest scales sampled by the Dynamics Explorer spacecraft at low altitudes (Weimer *et al.*, 1985). The FAST magnetometers thus have to provide information in both the large-scale/low frequency regime and the small-scale/high frequency regime.

2. Measurement Requirements

Factors influencing the dynamic range of magnetometer design are the need to measure the earth's full field as well as auroral structure down to arc scale-lengths. Thus field variations range from $\pm 65\,000$ nT through the largest scale currents ($\sim$1000 km) which typically cause deviations of several hundred nT at a few hundred kilometers altitude. At the smallest scales, Dynamics Explorer measurements indicate current-related structure down to a few nT. These extremes were discussed by Weimer *et al.* (1985), who showed electric and magnetic fluctuation amplitude as a function of equivalent wavelength down to about 5 km. The amplitude at this shortest wavelength is 3–5 nT; it is desirable to measure down to $\pm$ 2 nT to capture the smaller scale structure.

To resolve the smallest scale auroral current structures (100 m and less; cf., Borovsky (1995)), the field must be sampled at rates consistent with the convection of these structures past the spacecraft. Assuming a fastest-case convection speed (satellite plus arc motion, normal incidence) of 10 km s^{-1}, a structure of 100 m wavelength corresponds to a Nyquist frequency of 100 Hz, or a sample frequency of 200 Hz. Auroral zone ELF observations from Freja indicate background spectral densities of about 10^{-6} nT^2 Hz^{-1} at 80 Hz (between the O^+ and He^+ gyrofrequencies at Freja's altitude), and about 10^{-8} nT^2 Hz^{-1} near 1000 Hz (Erlandson *et al.*, 1994). Gurnett *et al.* (1984) have shown that low-altitude auroral zone magnetic spectral densities at 100 Hz are roughly 10^{-7} nT^2 Hz^{-1}, with a spectral slope much steeper than f^{-1}. At 100 Hz, background fluctuation amplitudes are about 1 pT. To study structures of 10-m scales, spectral densities below 10^{-10} nT^2 Hz^{-1} at 1 kHz must be measured.

Additional sensitivity requirements arise from the need to measure ion cyclotron waves, chorus and auroral kilometric radiation. The last is a stressing measurement objective, aimed at acquiring electromagnetic wave data at the lower end (several hundred kiloHertz) of the auroral kilometric radiation band.

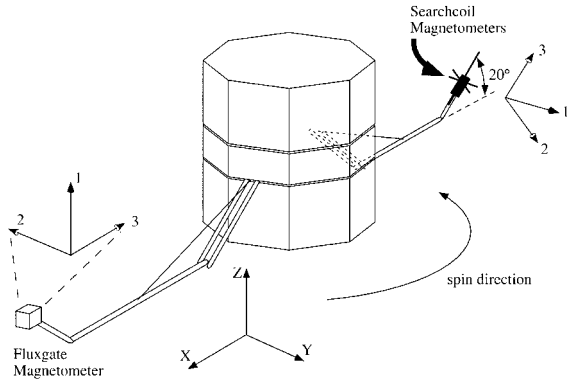

Figure 1. Schematic of the FAST DC fluxgate and AC searchcoil magnetometer mechanical configuration, as deployed in flight. See Pankow *et al.*, this issue, for details on the boom design.

3. Magnetometer Design

The necessary wide dynamic ranges in sensitivity and sampling frequency for FAST led us to use two techniques in magnetic field measurement. The background field, and large- and medium-scale field-aligned current signatures is most suited to a fluxgate magnetometer. For reasons made clear below, a search coil magnetometer is best for studying the higher frequency electromagnetic waves. This is primarily due to the sensitivity of the two designs at different frequency regimes; we intended that the two magnetometers overlap in frequency coverage.

The FAST triaxial fluxgate magnetometer heritage includes the OGO 5, ISEE 1 and 2, Pioneer Venus Orbiter, AMPTE UKS, and Galileo magnetometers, but it draws nearly all of its analog design from the Polar Magnetic Field Experiment (Russell *et al.*, 1995), so that development costs were kept to a minimum. Earth's large background field demands a range of $\pm 65\,000$ nT. With the use of a 16-bit, low mass, low power flight qualified analog-to-digital converter (ADC), we obtain a resolution of $\pm$ 2 nT, sufficient to resolve auroral current structures at large (100's of km) to small (1 km) scale. For a Nyquist frequency of 100 Hz, digitization noise is $(2\text{ nT})^2/12F_N = 3.3 \times 10^{-3}\text{ nT}^2\text{ Hz}^{-1}$. As discussed above, the level of natural signals can be several orders of magnitude lower. Consequently the useful fluxgate bandwidth at 16-bits resolution (for $\pm 65\,000$ nT) is from DC to about 20 Hz at FAST altitudes.

In order to measure electromagnetic waves and structures approaching the few tens of meters scale size, we use a triaxial search coil design. All three sensors cover the range from about 10 Hz to 16 kHz, and one of the three has a higher frequency response, out to 2 MHz to capture the low end of AKR. This approach provides overlap between the fluxgate and search coils at low frequencies. The triaxial design allows us to completely specify wave polarization and, with the electric field instrument, the Poynting flux of electromagnetic waves.

The deployed fluxgate and searchcoil mechanical configurations on FAST are shown in Figure 1. The three fluxgate sensors are sampled and digitized in the order shown; sensor 1 nominally points along the spin axis when the boom is properly deployed (see Pankow *et al.*, this volume), sensor 2 points opposite to the motion of the boom about the spin axis, and sensor 3 points back toward the spacecraft, along the boom. The fluxgate boom azimuth defines the X-axis of the spacecraft coordinate system.

The fluxgate magnetometer is a three axis instrument using highly stable low noise ring core sensors. The sensors are boom mounted approximately two meters from the spacecraft body, in a shielded housing $114 \times 54 \times 61$ mm in dimension. The sensors, housing, mounting bracket hardware and pigtail weigh 420 gm. The triaxial search coil magnetometer consists of two 7-inch (178 mm) sensors, and one 21-inch (533 mm) sensor mounted orthogonally. The 7-inch sensors have cores of laminated molybdenum permalloy, wrapped with a coil of 10 000 windings on a fiberglass bobbin. The 21-inch sensor consists of a laminated amorphous metal core laid in a fiberglass support structure, wrapped with a coil of 2000 windings on a fiberglass bobbin. One 7-inch sensor (sensor 1) is mounted so as to lie in the spin plane, the other (sensor 2) roughly antiparallel to the spin axis but canted outward from the spacecraft by 20°, and the 21-inch sensor (sensor 3) points approximately along the boom, but 20° up out of the spin plane. This mechanical configuration (see Figure 1) results from several constraints: (1) Mechanical stiffness and support during launch vibration is enhanced. (2) The 21-inch sensor fits within the Pegasus payload fairing. (3) The sensors have a full 2-m distance from the spacecraft following boom deployment. (4) The off-spin axis canting provides a measurement every spin of the vector AC magnetic field for higher frequencies, including AKR. The sensor assembly measures $533 \times 178 \times 178$ mm, with shielded pre-amplifiers located at the sensors, and weighs 707 g.

A single 251×257 mm circuit board contains the electronics needed to provide instrument clock, drive, sense and feedback to the fluxgate sensors, as well as Nyquist filtering of the analog voltages that are handed off to the switching and ADCs of the fields processor. This board also handles second stage amplification and filtering of the search coil signals, and hands them off to the fields switching/ADCs. It weighs 788 g. The entire analog magnetometer package consumes approximately 1.5 W.

Figure 2 is a block diagram of the analog magnetometer package. The fluxgate sensor electronics provide a 9 kHz drive signal for the sensors, a feedback signal which keeps the ring cores in zero field, and detect and amplify the second harmonic signals that are proportional to the ambient magnetic field. There is a 200 Hz low pass filter on the output, and the filtered result is provided to a switching system instead of a multiplexer (cf., Ergun *et al.*, this volume). This design provides greater isolation and less cross-talk between fluxgate channels; voltages settle better before being converted. The switching system output is provided to one of the fields experiment 16-bit ADCs (Ergun *et al.*, this volume). To simplify design

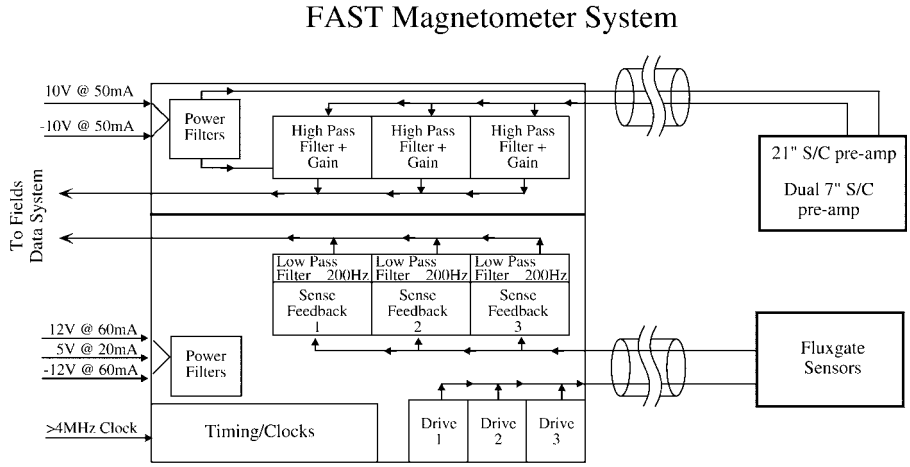

Figure 2. Block diagram of the analog DC and AC magnetometer package.

and reduce costs, the fields ADCs are generic, so the fluxgate data are sampled in the same way as electric field data. All searchcoil sensors are high-pass filtered to reduce the low-frequency AC signal due to the spinning main magnetic field. Data handling from the fields experiment ADCs are described in detail elsewhere (Ergun *et al.*, this volume).

4. Calibration

Initial ground calibration of the fluxgate magnetometer was complicated by noisy coils in the Goddard Space Flight Center magnetic calibration facility. Consequently, preliminary calibration was done on-orbit against the very well-characterized terrestrial field. This is considered adequate for FAST, since the thrust of the mission is to study field variations, not map the geomagnetic field to high accuracy and precision. The preliminary calibration resulted in a coupling matrix, which transforms data from sensor units in the non-orthogonal sensor system to geophysical nT quantities in the spinning spacecraft system. The preliminary coupling matrix is:

$$\begin{pmatrix} 0.984672 & 0.000000 & -0.008604 \\ 0.008272 & 0.928669 & -0.014153 \\ 0.006700 & 0.006234 & 0.957579 \end{pmatrix}.$$

The searchcoil sensors were calibrated on the ground in an end-to-end test using AC field stimulation by a solenoidal coil within a mu-metal flux can. The amplitude and phase relationship of the three sensors to the input signal was recorded at different frequencies. The two 7-inch sensors have peak measured sensitivities

of 1.9 V nT^{-1} Hz^{-1} at 8800 Hz, while the 21-inch sensor has a higher frequency response and greater peak sensitivity, 26.8 V nT^{-1} Hz^{-1} at 60 kHz. The detailed transfer functions of the search coil and fluxgate sensors are discussed below.

5. Command and Data Handling

Both the fluxgate and search coil instruments have single gain states; no ranging is required. Commanding involves providing power to the instruments, and in selecting the rate and type of data acquired in the fields package. The fastest fluxgate analog front-end sampling runs at a rate of 2048 samples s^{-1}, but at lower telemetry volumes, spot samples are taken at rates that are powers of 2 smaller, down to 16 samples s^{-1}. Following conversion, a digital recursive anti-aliasing filter is applied to the data, and the results are decimated by a factor of four (meaning that one in every four samples is kept). The output rate of the fields processor for DC fluxgate data are varied in different modes (see Ergun *et al.*, this volume) as required by survey and burst telemetry volume needs. The recursive filter ensures signal fidelity at the lowest telemetry rates during slow survey and non-auroral zone background data modes (output rates typically 4 or 8 samples s^{-1}). The fluxgate data are telemetered only as 16-bit waveforms, with output sample rates from as much as 512 samples s^{-1} down to 4 samples s^{-1}.

The fluxgate magnetometer sensors are sampled nearly, but not quite, simultaneously. The fields switching system samples sensor 1, then 2, then 3, then pauses a beat before starting again. The inter-sampling time is long enough to allow the voltage to settle, and is 5/16 of the overall sensor 1-2-3 sample cycle time. This basic sample rate, as described above, ranges from 2048 cycle s^{-1} down to 16 cycle s^{-1}, depending on fields data acquisition mode.

The digital recursive filter takes 1/16 of the current sampled magnetometer output from the ADC, and adds it to 15/16 of the previous filtered output value, and stores the result as the current output of the filter. These stored values have 20 bits of precision. When decimated by four and sent to the packetizer, they are truncated to 16 bits. The effective transfer function of the FAST fields processor data acquisition for the fluxgate magnetometer is

$$T(f) = (\tfrac{1}{15})/(\tfrac{16}{15} - e^{-i\pi f/4F_{No}}), \tag{1}$$

where f is frequency and F_N is the Nyquist frequency of the original (undecimated) samples, four times higher than the effective output Nyquist frequency. This is shown in Figure 3; the 3 dB point is at about 0.15 F_{No}, the output (decimated) Nyquist frequency. The fluxgate absolute frequency response depends on telemetry mode, and is summarized in Table 1; the recursive filter corner frequency (approximately the effective bandwidth) can be as low as ~0.2 Hz, and goes as high as ~22 Hz in some auroral fast survey modes.

TABLE I
FAST DC magnetometer bandwidth

Output sample Rate (sps)	Output Nyquist frequency F_{No} (Hz)	Filter Corner frequency (Hz)
512	256	21.8
256	128	10.9
128	64	5.45
64	32	2.72
32	16	1.36
16	8	0.68
8	4	0.34
4	2	0.17

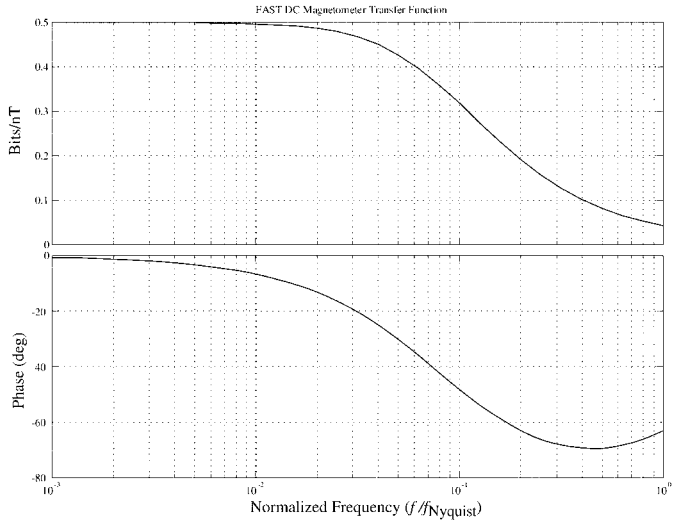

Figure 3. Effective transfer function of the DC magnetometer system. The transfer function is fixed to the output Nyquist frequency, which for FAST ranges from 2 to 256 Hz.

The search coil data are handled in several ways: waveform data are provided in survey mode at rates of from 32 to 2048 sample s^{-1} depending on telemetry mode, and in burst modes with 4-kHz bandwidth from all three sensors, and with 16-kHz bandwidth from the 21-inch sensor; high speed burst data result in waveforms with 1 MHz bandwidth from the 21-inch sensor; 512-point FFTs (from 0 to 16 kHz) of the 21-inch sensor data are performed by a DSP chip on orbit and passed down at various rates in specific packets; finally, swept frequency analyzer (SFA) data is captured with a bandwidth of 1 MHz. The searchcoil magnetometers are high-

pass filtered to attenuate the Earth's main field at the spin frequency. The corner frequencies of the filters are 1290 Hz for the 7-inch sensors and 201 Hz for the 21 inch sensor. The transfer function of the searchcoil magnetometers is shown in Figure 4a for the 4-kHz bandwidth burst quantities, and in Figure 4b for the 16-kHz bandwidth burst quantity from the 21-inch searchcoil. The 180° phase relationship at low frequencies results from a combination of the high-pass filter, which produces a 90° phase shift at frequencies well below the corner frequency, and the basic searchcoil response to $\partial B/\partial t$, another phase shift of 90° from B. Likewise, the sensitivity (bits nT^{-1}) increases as f^2 for frequencies below the high-pass corner frequency. Above this frequency, the phase moves toward the expected value of 90°, and sensitivity (bits nT^{-1}) goes up as f.

6. Data Reduction

Data reduction approaches depend on handling either waveform or spectral data. As described above, the output fluxgate sensor samples must be properly time-aligned, then deconvolved from the filter response, then orthogonalized and calibrated to geophysical units. The signal is reconstructed by interpolating the three missing values and then inverting the filter. This process necessarily amplifies any noise at higher frequencies, so we typically cut off the filter inversion at 10% of F_{No}, depending on the strength of the natural signal.

The searchcoil waveform data are samples taken at either 8192 or 32768 samples s^{-1}, depending on the burst waveform capture channel. The voltages digitized by the ADC are proportional to nT-Hz, and so must be calibrated taking into account the high-pass analog filter as well as the intrinsic linear gain in frequency. Pre-launch tests provided detailed transfer functions for the three sensors, and their response can also be checked on orbit by examining the amplitude and phase of the signal caused by the main field at the spin frequency. Waveform data are integrated first to recover from the high-pass filter, then again to transform from a voltage proportional to nT-Hz to nT.

Spectral data from the searchcoils undergo the same calibration on the ground, but this time in the frequency domain.

Attitude determination is critically important to reducing the magnetometer data. Spin axis pointing is controlled by a magnetotorquer which is activated as necessary near perigee, where magnetic fields are largest and the torque authority is greatest. Spin rate is maintained by a second magnetotorquer. Knowledge of spin axis pointing is determined roughly by means of a spinning sun sensor, which measures sun elevation angle and sun-crossing time. A much more refined spin axis pointing is obtained by using the measured magnetic field from a full orbit and comparing this to the IGRF 1995 model. Using a full orbit's worth of spin axis sensor measurements helps constrain the spin axis to a small fraction of a degree. The spinning sun sensor also provides absolute spin phase via a sun pulse when the

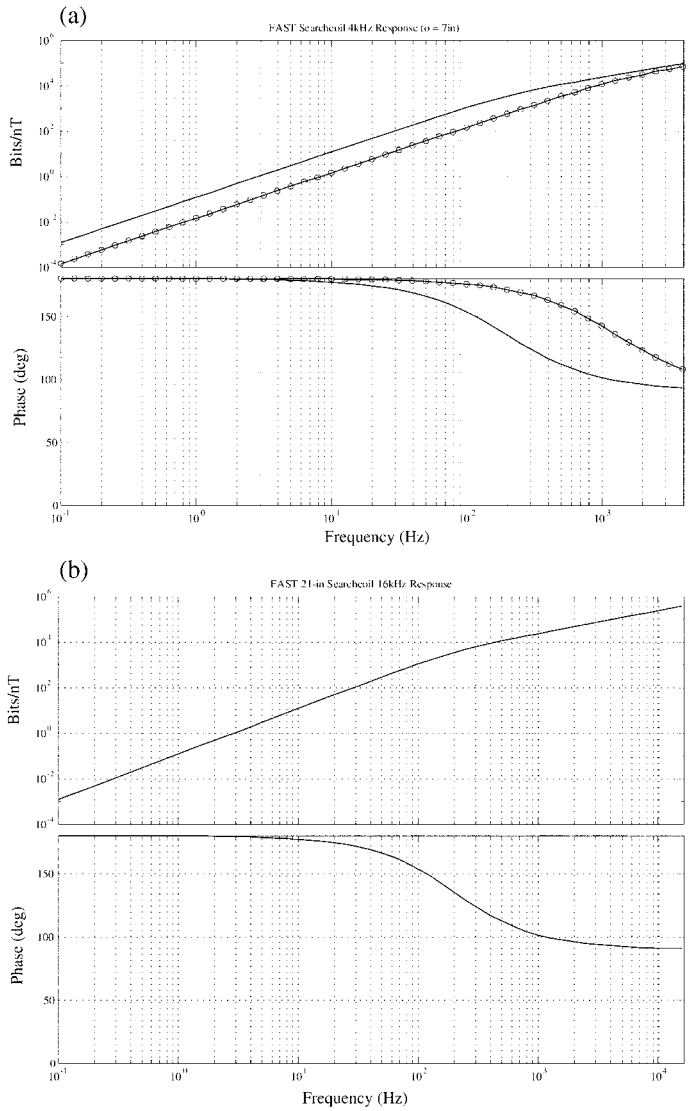

Figure 4. (a) Transfer function of searchcoils for the 4096-Hz bandwidth burst quantities. (b) Transfer function of the 21-inch searchcoil (Mag3ac) for the 16384-Hz bandwidth burst quantity.

satellite is in sunlight, while infrared horizon-crossing sensors provide coarser spin phase in eclipse. However, because of jitter in these pulse times the instantaneous absolute phase is poorly constrained. Consequently we smooth the roll phase but require it to pass through zero phase within a 'jitter window' of the nominal pulse time. This approach results in a smooth despinning process.

Relative gains and offsets for the spin plane sensors are obtained through a straightforward analysis of the DC and AC signals at the spin frequency performed

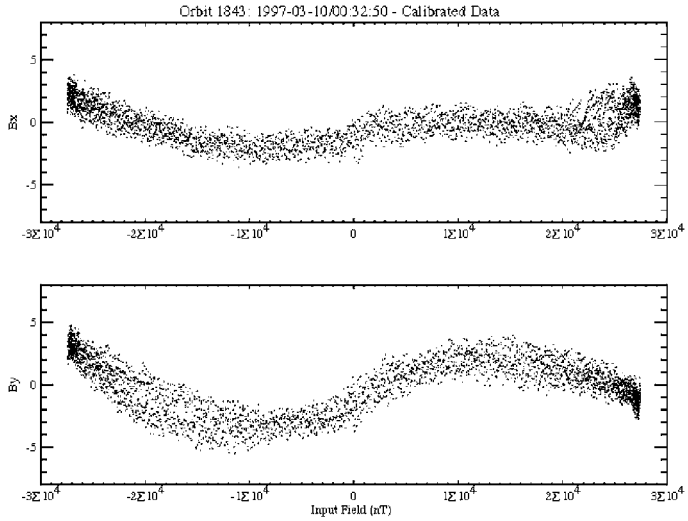

Figure 5. FAST fluxgate magnetometer nonlinearities. Shown here are the residuals from a sine wave fit to the X and Y axis data over several spins. The residuals show the sensor's departures from an ideal sine wave.

on every 2-spins worth (10 s) of data. The model used for each sensor is $(a_0 + a_1 t)\ \cos \omega t + (b_0 + b_1 t)\ \sin \omega t + c_0$, which allows for a linearly growing or decreasing background field amplitude over the 10 s interval, plus a constant value (offset + spacecraft field). Correlation of the spin plane sensor c_0 values with the spin axis field provides a measure of how much the spin plane sensors are canted out of the spin plane. A similar analysis of the spin axis sensor provides a measure of the off-spin cant angle. When this analysis is combined with the constraints of the IGRF model field, we can determine the parameters necessary to orthogonalize the sensors and determine absolute gains and offsets as well. Thus, adjustments to the relative calibration can be made smoothly every ~10 s as the data are processed. A correction for absolute calibration is obtained by comparing a full orbit of magnetometer data to the model field on *Dst* quiet days, about once a week.

7. Instrument Operation on Orbit

The fluxgate and searchcoil magnetometers have functioned normally for much longer than the nominal 1-year mission duration since turn-on in August of 1996. The boom deployment shortly after launch was flawless and placed the sensors in their nominal flight mechanical configuration.

The fluxgate magnetometer exhibits small departures from a linear response when spinning in Earth's main field at FAST's spin period of 5 s. The nonlinearities are first noticeable around 10 000 nT. Figure 5 shows the residuals from a sine

wave fit to the sensor data over two spins of the satellite, plotted as a function of the input field as modeled by the fit. The top panel shows the residuals for the X-sensor, sensor 3, the lower panel for the Y-sensor, sensor 2; a perfectly linear response would result in a flat line. The sensor 3 (MagX) response is linear within 2 nT out to about 10 000 nT, the overall departures from linear are about 3 nT in 30 000, or 10^{-4}. The sensor 2 response is somewhat worse, about 2×10^{-4}. We were also able to determine the spin axis sensor behavior before boom deployment (when the booms are stowed, sensor 3 is antiparallel to the spin axis, and sensor 1 lies parallel to the spin plane), and its nonlinear character was smaller than 10^{-4}. Since sensor 1 lies nearly along the spin axis after deployment, its spin frequency AC signal is much smaller than 10 000 nT, and its response is effectively linear. For the deployed spin plane sensors, the nonlinearities are not a problem because (a) they are small and (b) they are so systematic they can be easily removed with a simple function.

The fluxgate magnetometer boom undergoes very small, but detectable, changes in orientation over the course of an orbit. In Figure 6, we plot an orbit's worth of four quantities: the cosine and sine of the angle between the two spin plane sensors (TW_YX, TW_YY) multiplied by the gain ratio of the two sensors (ideally unity), and the angles between the spin axis sensor and the X spin plane direction (TW_ZX) and the Y spin plane direction (TW_ZY). The first two quantities describe how the spin plane sensor mechanical mounting and/or electronic cross-talk change over the course of an orbit; the second two quantities provide similar information on mounting/cross-talk for the spin axis sensor, but also provide some measure of boom flexure and torsion. The satellite leaves eclipse at about 07:27 UT, moves across Earth's dayside toward perigee at about 09:00 UT, and enters eclipse again around 09:04 UT. At eclipse exit, there is little or no change in the spin plane sensors alignment/cross-talk, but there is a rapid change in TW_ZX from 0.3 milliradians to 0. At the same time, TW_YX exhibits no rapid change but begins a gradual trend from 0 to 0.5 mradians over about 20 min. These diagnostics indicate that there is a very prompt response ($\tau < 2$ min) by the magnetometer boom to the sunlight/eclipse transition, and a longer time-scale ($\tau \sim 20$ min) for torsion or twisting of the boom. Since these diagnostics are obtained by detailed analysis of the spin frequency signals on all three axes, it might be argued that some of the apparent spin axis sensor changes at eclipse entry and exit are due to a signal caused by solar array currents flowing while the satellite is in sunlight. Such currents would produce, to lowest order, a spinning dipole field as seen by the magnetometer sensors. However, such a contribution would be roughly constant in amplitude, while the signal we observe is instead a constant fraction of the magnitude of the spin plane field, and hence is an angular displacement. It can be seen that a change of similar size in TW_ZX but of opposite sign takes place as the satellite moves from sunlight to shadow at around 09:04 UT. A change in the apparent zero level of the X spin plane sensor (which should be proportional to the

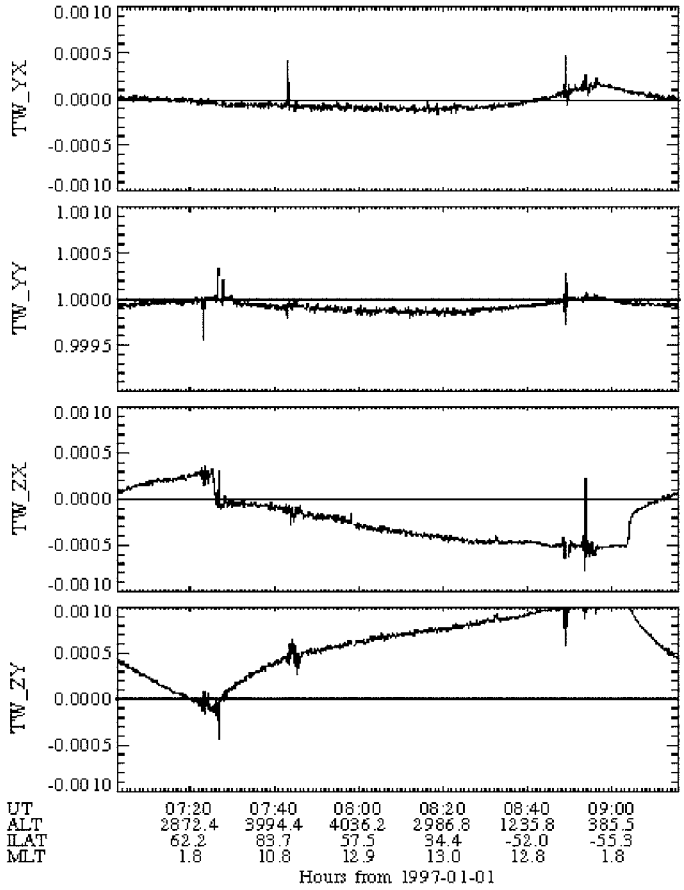

Figure 6. FAST fluxgate magnetometer orthogonality diagnostics, showing small changes in sensor and/or boom orientation with respect to the spin axis and spin plane over the course of an orbit. Exit from eclipse is at 07:27 UT, entry is at 09:04 UT, a few minutes after perigee. The diagnostics indicate that boom flexure and torsion are small but detectable, in the 0.3–0.5 mradian range (0.02° –0.04°).

change in the sensor's out-of-spin-plane angle) confirms that this is a boom flexure effect.

The FAST spacecraft is magnetically very clean. Except when the torque coils are operating, spacecraft fields are negligible. In any case we cannot distinguish between spacecraft fields and the intrinsic magnetometer offsets, which are fairly small and stable. The sum of offsets and spacecraft fields vary slowly with time, and exhibit a mild temperature dependence. The torque coils, which operate infrequently, create fields at the fluxgate of about 500 nT. The only AC interference observed by the searchcoils is the fluxgate drive frequency at 9 kHz, and this signal is at a low level.

8. Science Results

One issue which is central to auroral physics specifically and magnetosphere/ionosphere coupling in general is how and where field-aligned currents close through the ionosphere and in the magnetosphere. FAST is uniquely suited to studying auroral microprocesses, but the particles and fields instruments also address questions of a more global nature, like the closure of field-aligned currents (FACs). Of course, FACs have been observed and studied by rockets and satellites for decades - the new observations which FAST brings to the discussion are high sensitivity, high time resolution plasma measurements with continuous monitoring of all pitch angles, and high time resolution measurements of fields.

The FAST fluxgate magnetometer observes small-scale regions of downward-going current within the large-scale field-aligned current regions of the auroral zone. Associated with these downward currents are upward flowing low- and medium-energy (up to about 1 keV) electron beams. The scale size of the downward currents can be kilometers or less, often concentrated at the edges of inverted-V structures. These upgoing electrons have occasionally been observed before (Boehm *et al.*, 1995; Clemmons *et al.*, 1995), but the FAST instrumentation allows continuous high-time-resolution monitoring of particle distribution functions. The upgoing accelerated electrons/downward currents are also associated with diverging electric fields, and presumably with the 'black aurora', the optical counterpart of bright discrete arcs (Marklund *et al.*, 1994, 1997a, b). FAST data taken at apogee (4000 km) and near magnetic midnight commonly show downward FACs with current densities of between 2 and 4 microamps per square meter, consistent with the observed upward flux of $\sim 10^9$ electrons $cm^{-2}\ s^{-1}$.

Figure 7 shows DC magnetic field and electron plasma analyzer data. The field data have been detrended using the model field, IGRF 1995, but are in despun spacecraft coordinates, with the top panel corresponding to most of the main field. The second panel shows the north-south excursions, and the third the east-west excursions – all to the same scale. The plots go from lower latitudes to higher latitudes, starting at about 67° ILAT and ending at about 73°. A positive excursion of ΔB_{EAST} corresponds to a downward current, a negative excursion to an upward current.

The bottom two panels show the electron energy spectrum between 5 eV and about 30 keV, summed over all pitch-angles, and the electron pitch-angle spectrum summed over all energies. 0° and 360° correspond to field-aligned, or downgoing electrons, while 180° is upgoing from the ionosphere. One can see the atmospheric loss cone between roughly 150 and 210°.

At lower latitudes, roughly isotropic plasma sheet electrons are observed, which at higher, sub-auroral latitudes are interspersed with upgoing accelerated electron beams. Each beam interval is associated with an increase in ΔB_{EAST}, corresponding to a downward FAC. Then FAST passes into the auroral acceleration region proper, with inverted-V structure, lasting about a minute during which the space-

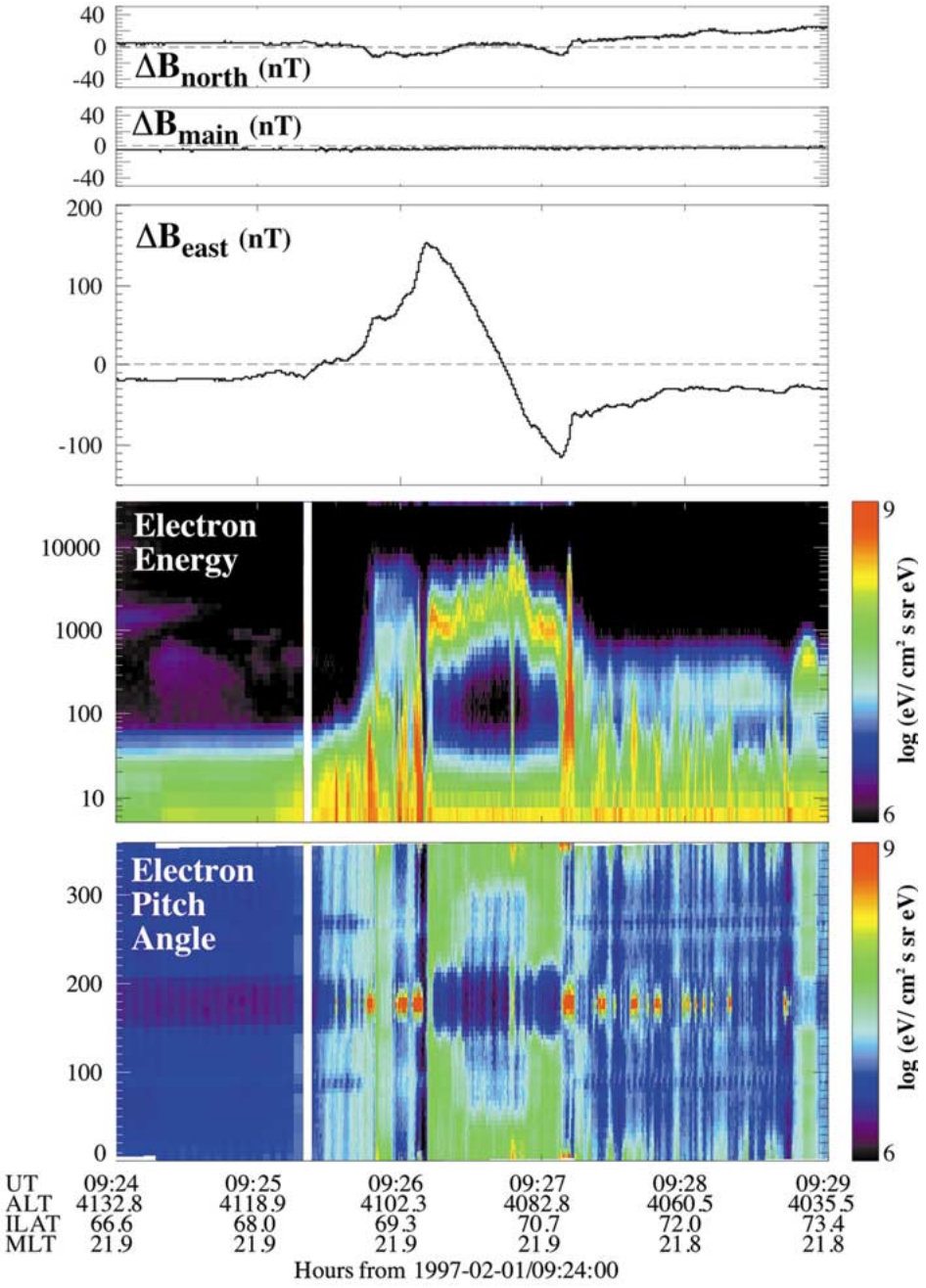

Figure 7. FAST fluxgate magnetometer and electron electrostatic analyzer data from a pre-midnight auroral zone pass on February 1, 1997. The magnetometer data have been detrended with IGRF 1995, but are in spacecraft coordinates – the top panel is essentially directed to the north, the second and third panels correspond to the main-field and east-west directions, respectively. The fourth and fifth panels are electron energy (over all pitch angles) spectra and electron pitch-angle (over all energies) spectra. Upward electron beams can be seen at pitch angles of 180°, and these correspond to positive deflections in the ΔB_{EAST} component, consistent with passage through downward field-aligned currents.

craft moves roughly 360 km. The field perturbation in this region is all upward FAC, as one would expect. This is followed by a brief but very intense upgoing electron beam, with energies going up to nearly 10 keV. The total downward current found equatorward and poleward of the inverted-V region just about balances the upward current carried by auroral precipitation, and by the time FAST has gone up to 73° the perturbation field has returned to nearly its starting point, indicating that little net current was flowing into or out of the auroral ionosphere on this occasion at this local time. Conditions for this interval were quiet, and the interplanetary field based on WIND key parameters was northward. Figure 8 displays some of the fields wave data products created onboard FAST (see Ergun *et al.*, this volume). Here we focus in on the AC electric and magnetic field observations within the primary auroral acceleration region for another FAST premidnight northern winter pass. Once again FAST is flying from lower latitudes to high, this time close to 23 MLT. The top panel shows the eastward magnetic field component, while the second and third panels provide the electron energy and pitch angle spectrograms that place the currents and waves in context. The next four panels are, respectively, high- and low-frequency spectrograms of the electric and magnetic field wave activity. High frequency in this case refers to the swept frequency analyzer data between roughly 10 kHz and 2 MHz, and the low frequency denotes the 16 Hz to 16 kHz DSP fourier analysis. The SFA spectrograms show the presence of auroral kilometric radiation near roughly 300 kHz, while the DSP spectrograms display a combination of VLF saucers, VLF hiss, ion cyclotron waves and lower hybrid emissions.

At about 20:50:10 UT, FAST was observing precipitating electrons with energies near 10 keV, carrying an intense upward FAC (note the steep negative slope in B_{east}), and collimated beams of upward-going ions (not shown) with energies of several keV. This situation obtains when the parallel accelerating potential is partly above and partly below the satellite. Within this interval, emissions at the hydrogen cyclotron frequency near 200 Hz can be seen in the electric and magnetic field DSP spectrograms. Figure 9 focuses in on a short period of time, 20:50:09.927–20:50:10.176 UT (denoted by the black vertical line in Figure 8), within one of the inverted-V's of the primary auroral acceleration region. Shown here are the 4096-Hz bandwidth waveforms from the three searchcoil sensors (see Figure 1) and the electric field (cf., Ergun *et al.*, this volume). The clearest signal is the ∼200-Hz H^+ cyclotron frequency emission. Searchcoil sensors 1 and 2 were oriented at about 90° to the main magnetic field at this time, while sensor 3 was oriented roughly within 20° of the field. Consequently the difference in amplitudes at the three sensors is likely related to the polarization of the magnetic part of the wave. There are also lower-frequency fluctuations in sensors 1 and 2 that roughly correspond to the gyrofrequency of O^+ at ∼12 Hz; but with amplitudes of ∼1 nT, these waves would be at about the 7-inch searchcoil digital noise level near 10 Hz (see Figure 4(a)). Moreover, there is little counterpart signal at ∼12 Hz in either the more sensitive 21-inch searchcoil (sensor 3) or the electric field waveform.

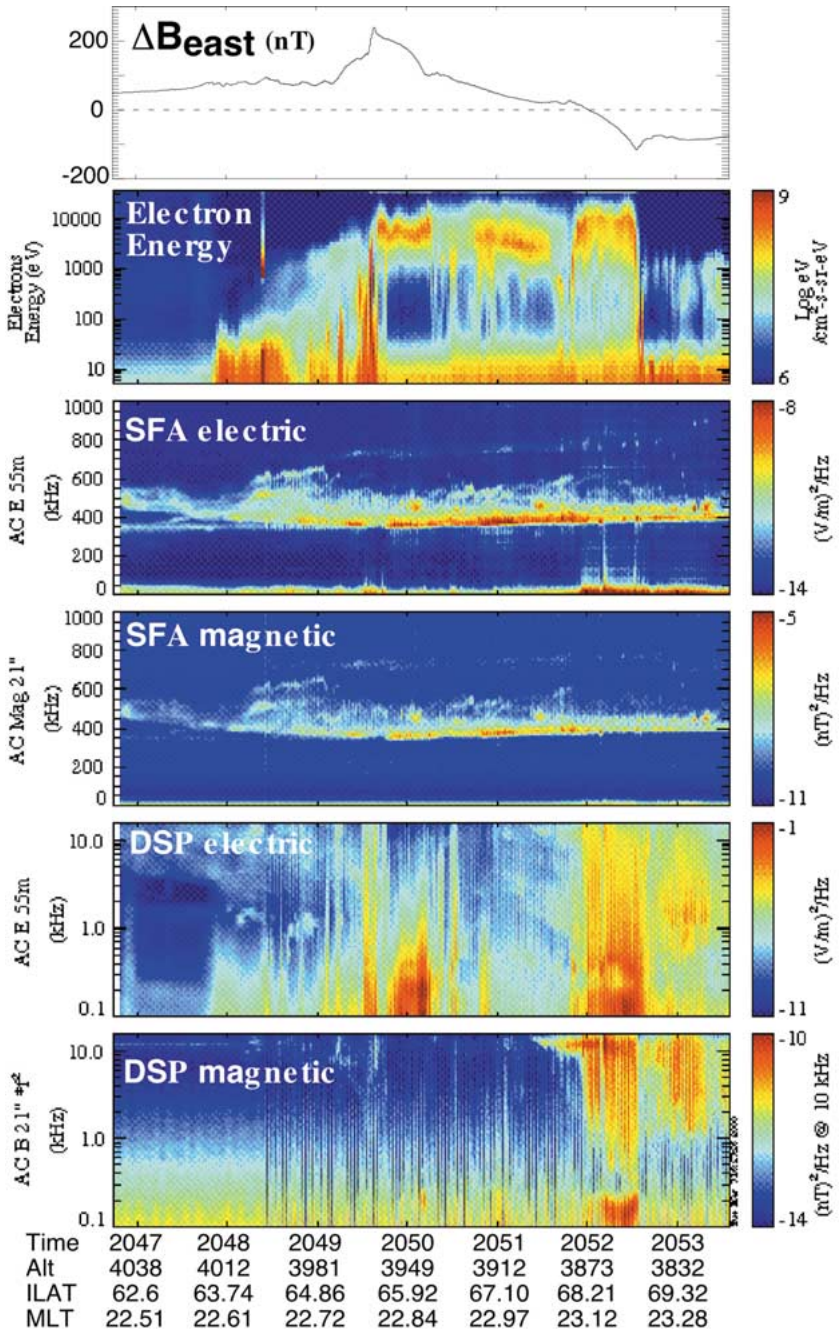

Figure 8. FAST ΔB_{EAST} magnetic field component, electron energy spectrum, and electric and magnetic SFA and DSP wave spectrograms for a pass on February 7, 1997. The electric and magnetic components of auroral kilometric radiation can be seen near 300 kHz in the SFA spectrograms. The DSP spectrograms display VLF saucers, hiss and ion cyclotron emissions.

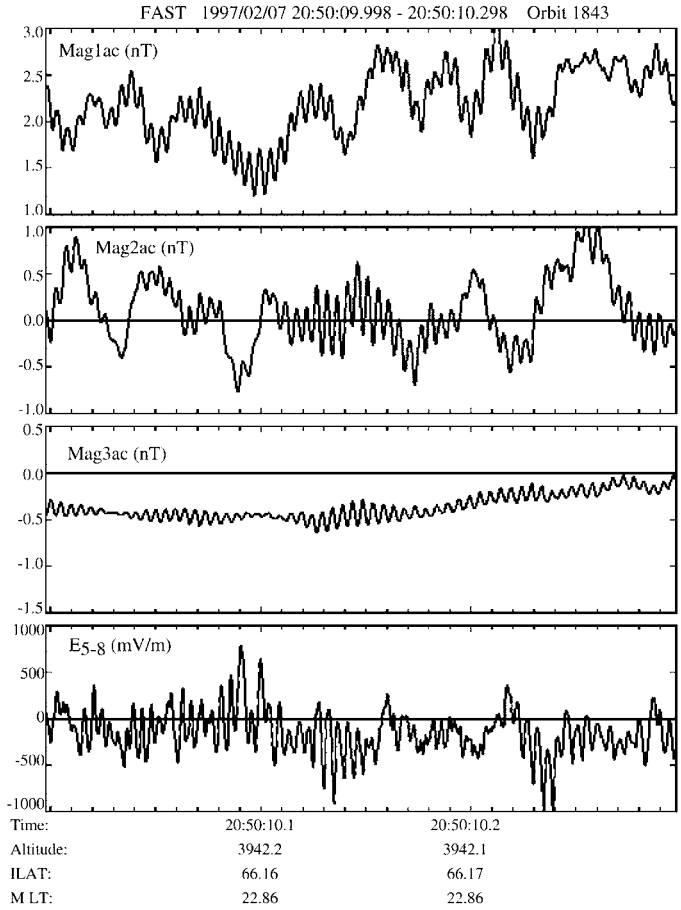

Figure 9. FAST 4096-Hz bandwidth waveform data for the three searchcoil sensors and the electric field for a period of about 250 ms from Figure 8. The principal feature is a hydrogen cyclotron emission at ∼200 Hz.

9. Summary

The FAST magnetometer investigation consists of a tri-axial fluxgate magnetometer to measure DC and ULF fields (0−∼20 Hz), and three searchcoil magnetometers to measure AC magnetic fields from around 10 Hz to 2 MHz. This implementation allows magnetic field coverage from the largest fields and lowest frequencies to the small plasma wave fields at high frequencies. Sensitivities range from 2 nT bit^{-1} at DC to greater than 3 fT bit^{-1} at 16 kHz. The combined magnetic fields instruments, including both fluxgate and searchcoil sensor sets, pigtails and analog board, weighs about 1.9 kg, and consumes about 1.5 W of power. The digitization of the output signals, and subsequent signal processing, are handled by a central FAST fields processor (see Ergun *et al.*, this volume), which makes

sure that both E-field and B-field quantities are precisely timed and co-sampled to facilitate intercomparison. The instruments have been operating nominally on orbit since launch in August 1996.

Acknowledgements

This work was supported by NASA order number S-57795-F. We are grateful to the FAST team for comments and suggestions.

References

Boehm, M. H., Clemmons, J. H. Wahlund, J -E., Eriksson, A., Eliasson, L., Blomberg, L., Kintner, P., and Höfner, H: 1995, 'Observations of an Upward-directed Electron Beam with the Perpendicular Temperature of the Cold Ionosphere', *Geophys. Res. Lett.* **22**, 2103.

Borovsky, J. E.: 1993, 'Auroral arc Thicknesses as Predicted by Various Theories', *J. Geophys. Res.* **98**, 6101.

Clemmons, J. H., Boehm, M. H., Blomberg, L. G., Wahlund, J. -E., Eliasson, L., Lühr, H., and Haerendel, G.: 1995, 'Upwardly Accelerated Auroral Electrons: The Role of Parallel Electric Fields' (Abstract), *EOS Trans. Am. Geophys. Union* **76**, F551.

Erlandson, R. E., Zanetti, L. J., Acuña, N. H., Erksson, A. I., Elliasson, L., Boehm, M. H., and Blomberg, L. G.: 1994, 'Freja Observations of Electromagnetic Ion cyclotron ELF Waves and Transverse Oxygen Ion Acceleration on Auroral Field Lines', *Geophys. Res. Lett.* **21**, 1855.

Gurnett, D. A., Huff, R. L., Menietti, J. D., Winningham, J. D, Burch, J. L., and Shawhan, S. D.: 1984, 'Correlated and Low-Frequency Electric and Magnetic Noise Along the Auroral Field Lines', *J. Geophys. Res.* **89** 8971.

Marklund, G: 1997, 'Auroral Phenomena Related to Intense Electric Fields Observed by the Freja Satellite', *Plasma Phys. Control. Fusion* **39**, 195.

Marklund, G., Karlsson, T., and Clemmons, J.: 1997, 'On Low-Altitude Particle Acceleration and Intense Electric Fields and their Relationship to Black Aurora', *J. Geophys. Res.* **102**, 17 509.

Marklund, G., Blomberg, L., Fälthammar, C.-G., and Lindqvist, P. -A.: 1994, 'On Intense Diverging Electric Fields Asociated with Black Aurora', *Geophys. Res. Lett.* **21**, 1859.

Russell, C. T., Snare, R. C., Means, J. D., Pierce, R. D., Dearborn, D., Larson, M., Barr, G., and Le, G.: 1995, 'The GGS/Polar Magnetic Fields Investigation', *Space Sci. Rev.* **71**, 563.

Sugiura, M., Maynard, N. C., Farthing, W. H., Heppner, J. P., and Ledley, B. G.: 1982, 'Initial Results on the Correlation Between the Magnetic and Electric Fields Observed from the DE-2 Satellite in the Field-Aligned Current Regions', *Geophys. Res. Lett.* **9**, 985.

Weimer, D., Goertz, C. K., Gurnett, D. A., Maynard, N. C., and Burch, J. L.: 1985, 'Auroral Zone Electric Fields from DE 1 and DE 2 at Magnetic Conjunctions', *J. Geophys. Res.* **90**, 7479.